Int. J. Electrochem. Sci., 15 **(2020)** 4242 – 4251, doi: 10.20964/2020.05.63

International Journal of
ELECTROCHEMICAL
SCIENCE
www.electrochemsci.org

Metal-Organic Framework-derived synthesis of MoO_2-Cu@NC nanocomposites for enhanced lithium storage properties

Zhenghao Liu, Mengzhi Yao, Yourong Wang, Youcai Liang, Yuhan Li and Siqing Cheng**

Innovation Center for Nanomaterials in Energy and Medicine (ICNEM)
School of Chemical and Environmental Engineering, Wuhan Polytechnic University, Hubei 430023, P. R. China
*E-mail: wyourong@163.com

Received: 5 January 2020 / *Accepted:* 10 February 2020 / *Published:* 10 April 2020

As advanced electrode materials for lithium ion batteries, the application of molybdenum dioxide (MoO_2) is hampered by poor cycle stability and rate performance. In this work, a novel Mo/Cu metal organic framework (MOF) has been synthesized using nitrogen-rich folic acid (FA) as an organic ligand through liquid-phase method for the first time at room temperature. After a simple annealing treatment, MoO_2-Cu@nitrogen-doped carbon (NC) nanomaterials derived from the Mo/Cu based MOF were obtained, which exhibit excellent performance as the anode material for lithium-ion batteries. The reversible discharge capacity of MoO_2-Cu @NC nanocomposites exceeds 1000 mAh g^{-1} at 100 mA g^{-1}, which remains 846 mAh g^{-1} after 100 cycles. Meanwhile, the obtained MoO_2-Cu@NC nanocomposites also show good rate performance (580 mAh g^{-1} at 1000 mA g^{-1}).

Keywords: Metal organic framework (MOF); MoO_2; Folic acid; Lithium ion batteries

1. INTRODUCTION

With the growing demands for energy and the strong call to reduce carbon emissions, the innovation has become a research hotspot in energy storage devices over the past few decades [1, 2]. Among clean energy devices, lithium-ion batteries have been considered to be attractive energy sources for electric transportation and portable electronic devices because of high energy density, a low decrease in capacity when not in use and no memory effect [3-5]. However, due to the low theoretical capacity, the developments of advanced LIBs are hindered by the commercial graphite electrodes. Consequently, it is necessary to develop novel high-capacity alternative electrode materials [6, 7].

Transitional metal oxides (TMOs) have become attractive candidates for their high theoretical specific capacity [8]. The high-energy advantages of TMO electrodes are mainly due to their full utilization for redox reactions involving multiple electrons with lithium[9, 10]. As a representative transition metal oxide (TMO), MoO_2 has attractive properties such as high theoretical capacity (838 mAh g^{-1}) and low resistivity (8.8×10^{-5} Ωcm at 300 K in bulk samples), natural abundance and environmentally friendly nature [11], so it is considered to be promising anode material. Therefore, the application of MoO_2 based materials in lithium-ion battery has been widely explored in recent decades [12]. Nonetheless, the volume change and particle aggregation for MoO_2 materials during charge/discharge process cause serious cycling problem and huge capacity loss[13, 14].

To address these issues, one common strategy is to construct nanostructured MoO_2, such as nanoparticles [15], nanorods [16], nanosheets [17] and nanotubes [18], as it maximizes the contact surface area between the electrode and electrolyte. It also shortens the diffusion path of electrons and lithium ions, thereby improving the electrochemical performance. Nevertheless, due to volume changes during lithium insertion and extraction, nanostructured materials are still subject to capacity degradation over long periods of time. Surface modified carbon is another effective strategy to improve the electrochemical performances of MoO_2 electrode. Carbon coating not only relieve the volume changes of active materials, but also enhances the electrical conductivity, thereby improving the reversibility and cycle performance of charge and discharge [19, 20].

In recent years, transitional metal oxide/carbon composites achieved through thermal decomposition of metal-organic frameworks have attracted considerable attention because of their unique structural features [21, 22], as well as wide applications in catalysis [23] and lithium ion batteries [24, 25]. However, there are only a few reports on using metal-organic frameworks as a precursor to prepare MoO_2/C composites for lithium ion batteries [26]. Chen group synthesized porous MoO_2@C nano-octahedrons through directly calcinating the POMOF (NENU-5) precursor, which show superior capacity and stability (1442 mA h g^{-1} after 50 cycles at 100 mA g^{-1} [27]. The MOF derived hollow MoO_2/C shows reversible capacities up to 810 mA g^{-1} even after 600 cycles at 1000 mA g^{-1} [28]. Nevertheless, the organic linker of MOF derived from MoO_2/C reported in the literature is only limited to 1, 3, 5-benzenetricarboxylic acids. The nitrogen-doped carbon can improve conductivity and enhance reaction kinetics. Therefore, the MoO_2/N-C spheres have a reversible high specific capacity of 899 mAh g^{-1} at the current of 100 mA g^{-1} , improved rate capability and cycling performance [29]. In addition, the Cu nanoparticles are evenly dispersed in carbon skeleton to form a conductive network for fast charge transfer [30].

Inspired by above-mentioned strategies, herein, we explored a novel strategy using nitrogen-rich folic acid (FA) as an organic ligand to synthesize Mo/Cu based MOF by liquid phase method at room temperature for the first time, which were converted into MoO_2-Cu@NC nanocomposites after a thermal treatment. When used as lithium storage electrodes, the obtained MoO_2-Cu@NC nanocomposites offered a high reversible capacity and excellent cycle stability.

2. EXPERIMENTAL SECTION

2.1. Materials preparation

All reagents were of analytical grade and used without being purified. Mo/Cu-MOF was synthesized by liquid phase method at room temperature. In a typical synthesis, 0.2 g of Cu

$(CO_2CH_3)_2 \cdot H_2O$, 0.08 g of l-glutamic acid and 0.3517 g of ammonium molybdate tetrahydrate were dissolved in a certain amount of deionized water to form an uniform solution A with stirring for 30 min, 0.2682g 97% folic acid was dissolved in 40ml ethanol solution to form an uniform solution B with stirring for 2 hours. Then solution A was added dropwise to the solution B and a green precipitate appeared immediately. The green precipitates were collected by centrifugal after being stirred at room temperature for 14 hours, washed with ethanol for several times and then were dried at 60 ℃ for 12 hours to obtain Mo/Cu-MOF.

To prepare MoO_2-Cu@NC nanocomposites, Mo/Cu-MOF was placed in a tubular furnace, and then heated to 600℃ and maintained at this temperature for 2.0 h under argon gas flow. Finally, the MoO_2-Cu@NC nanocomposites were obtained.

2.2 Material characterization

FTIR spectra were recorded on 330 FT-IR Thermo Nicolet instrument in the 4000–400 cm^{-1} region. Thermogravimetric analysis (TGA) was carried out with a TA-Q600 instrument in a nitrogen atmosphere at a heating rate of 10 ℃ min^{-1}. The crystalline phases of samples were determined by a Shimadzu XRD-7000 X-ray diffractmeter (XRD) with Cu Kα irradiation at a scanning rate of 6° min^{-1}. Raman spectra were performed using a DXR Raman spectrometer (Thermo Inc. America) with a laser line of 532 nm. The morphology was investigated by field-emission scanning electron microscopy (FESEM, JSM-7100F). The obtained sample was characterized by a CHN elemental analyzer (an Elemental analyzer Vario EL cube). The contents of Cu and Mo were measured by an atomic emission spectrometer (ICP, Agilent ICPOES 720). Types and contents of component elements in the Micro region of the sample were recorded on an Energy Dispersive Spectrometer (EDS, INCA X-MAX 250).

2.3 Electrochemical measurements

The active material, superconducting carbon and polyvinylidene fluoride were mixed to prepare uniform slurry at the mass ratio of 7:2:1. Then the copper foil (collector) with size of 1 cm ×1 cm was made. After pasting the above slurry on the copper foil (collector), the working electrode was dried at 80 °C for 24 h in a vacuum oven. The batteries were assembled in a glove box under an inert atmosphere with Li foil as the reference and counter electrode, Celgard (2300) as the separator and 1M $LiPF_6$ solution in ethylene carbonate (EC)/dimethylcarbonate (DMC)/diethyl carbonate (DEC) (1 : 1 : 1 in volume) as the electrolyte. The galvanostatic cycling tests of the electrode were carried out using CR2016 coin cells via a battery cycle testing system (Land CT2001A, China) with the charge-discharge voltage range from 0.01 to 3.0 V (vs. Li^+/Li). The electrochemical impedance spectroscopy (EIS) was measured by an electrochemical work-station (CHI660C, China) in the range of 0.1Hz~1.0 × 10^5 Hz. Cyclic voltammetry (CV) were obtained on an electrochemical workstation (CHI660C, China) from 0.0–3.0 V (vs. Li^+/Li) at a scanning rate of 0.2 mV s^{-1}.

3. RESULTS AND DISCUSSION

FTIR spectra of folic acid and Mo/Cu-MOF were recorded on 330 FT-IR Thermo Nicolet instrument in the 4000–400 cm^{-1} region, as shown in Fig. 1a.

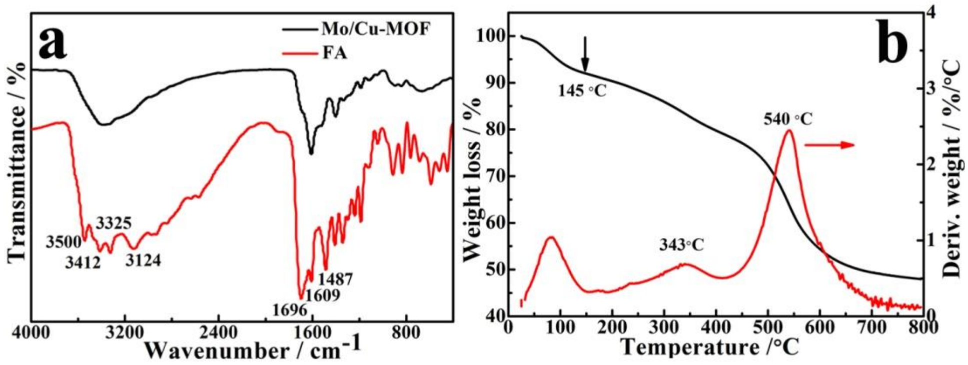

Figure 1. (a) FTIR spectrum of Mo/Cu-MOF and FA and (b) TGA-DSC curves of Mo/Cu-MOF nanocoposites in N_2

The main characteristic peaks of FA include 1609 cm^{-1} for NH bending vibration, 1487 cm^{-1} for CH_2 bending vibration, 1696 cm^{-1} for the C=O stretching vibration, and 3200–3500 cm^{-1} for the NH stretching vibration in NH_2 and amide NH groups. However, in the FTIR spectrum of Mo/Cu-MOF, most peaks disappeared or weakened in comparison with FA, which might indicate that the organic functional group in FA could be embedded into the internal cavities of Mo/Cu-MOF [31]. Especially, no peak at 1696 cm^{-1} was detected, suggesting the coordination of C=O in -COOH and the molybdenum/copper [32].

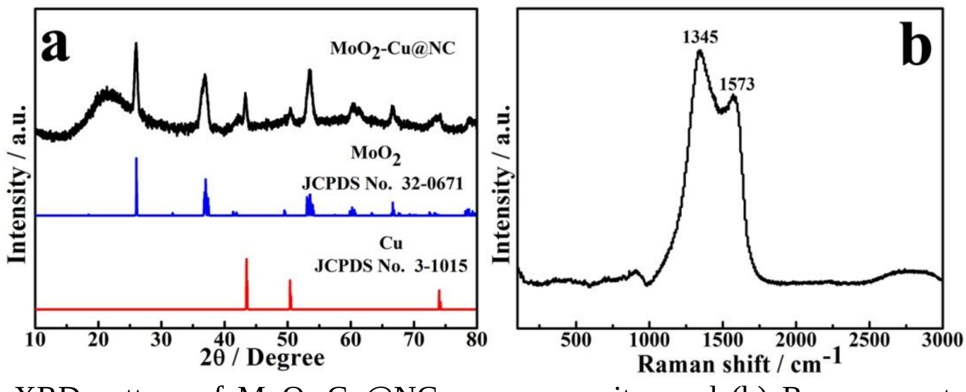

Figure 2. (a) XRD pattern of MoO_2-Cu@NC nanocomposites and (b) Raman spectrum of MoO_2-Cu@NC nanocomposites

Thermogravimetric analysis showed that the Mo/Cu-MOF underwent a weight loss of 8.03% from room temperature to 145 ℃, which is equivalent to the loss of all water molecules. When the experimental temperature was further increased, significant weight loss can be observed at about 343 and 540 ℃, indicating the decomposition of Mo/Cu-MOF. During the annealing process, MoO_2

formed. Meanwhile, a carbon matrix is obtained from FA ligands and Cu^{2+} is reduced to Cu. However, when the degradation temperature is further increased, MoO_2 react with carbon to form molybdenum carbide [28]. Therefore, the degradation temperature is kept at 600 ℃ for 2 h to obtain MoO_2-Cu@NC nanocomposites.

The crystallographic structure of MoO_2-Cu@NC nanocomposites is characterized by XRD analysis. It can be seen from Fig.2a that the main diffraction peaks can be indexed to the monoclinic MoO_2 phase (JPCDS card no. 32-0671). While diffraction peaks widen suggest that the MoO_2 particles is at the nanoscale, which is caused by the carbon matrix barrier [33]. Three peaks are observed at 43.4 50.4, and 74.1, which is indexed to the crystal planes of Cu phase (JCPDS no. 3-1015), respectively. The peak from carbon is barely visible due to its amorphous nature. The carbon structure was characterized using Raman spectroscopy and the results are shown in Fig. 2b. Two peaks can be seen clearly from Fig. 2b. The peak at 1573 cm^{-1} (G-band) is usually associated with the vibration of sp2 carbon atoms of the ordered carbon. The peak at 1345 cm^{-1} is usually related to the vibrations of disordered carbon (D band).This confirms the existence of carbon in MoO_2-Cu@NC nanocomposites. It is a common sense that the intensity ratio of D to G bands was used to characterize the structural order of carbon materials [34-36]. The intensity ratios of the D to G band (I_D/I_G) are 1.25, which are higher than those of other reported carbon materials [15, 37]. This result demonstrates that the degree of graphitization of carbon is lower because of the low synthesis temperature. Moreover, higher I_D / I_G values indicate more defects and disorder, which is beneficial to enhance the electrical and ionic transport of the electrode [9].

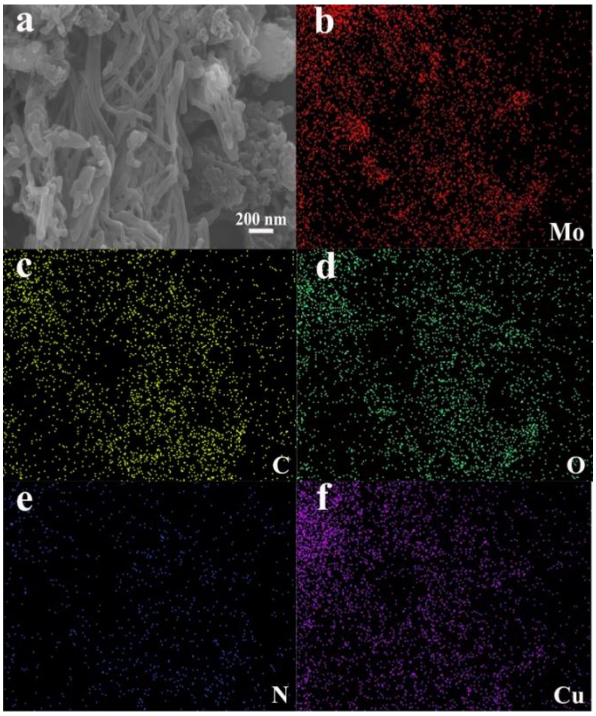

Figure 3. FESEM images and elemental mapping images of MoO_2-Cu@NC nanocomposites

The morphology of the MoO_2-Cu@NC nanocomposites is investigated by FESEM, which is displayed in Fig. 3a.The image reveals that the synthesized MoO_2-Cu@NC nanocomposite has a nanorod shape. MoO_2-Cu@NC nanorod is about several micrometers in length and 100 nm in diameter. The nanorods are decorated with nanoparticles. The FESEM-EDX elemental mapping images are shown in Fig. 3b-f. The images show that Mo, C, O, N and Cu elements are well distributed in the synthesized MoO_2-Cu@NC nanocomposites. In order to determinate the composition of MoO_2-Cu@NC nanocomposites accurately, the CHN element analysis and ICP measurements were also done. The content of C, H, N elements is 24.55, 1.18 and 6.04 wt% on element analysis, respectively. The results of ICP give percentage ratio of Cu, Mo element, which is about 26.7 wt% and 23.75 wt% in the prepared nanocomposites, respectively. MoO_2 content is about 31.67 wt% according to the calculation of Mo percentage ratio. All test results demonstrate that the MoO_2-Cu@NC nanocomposites have been successfully synthesized.

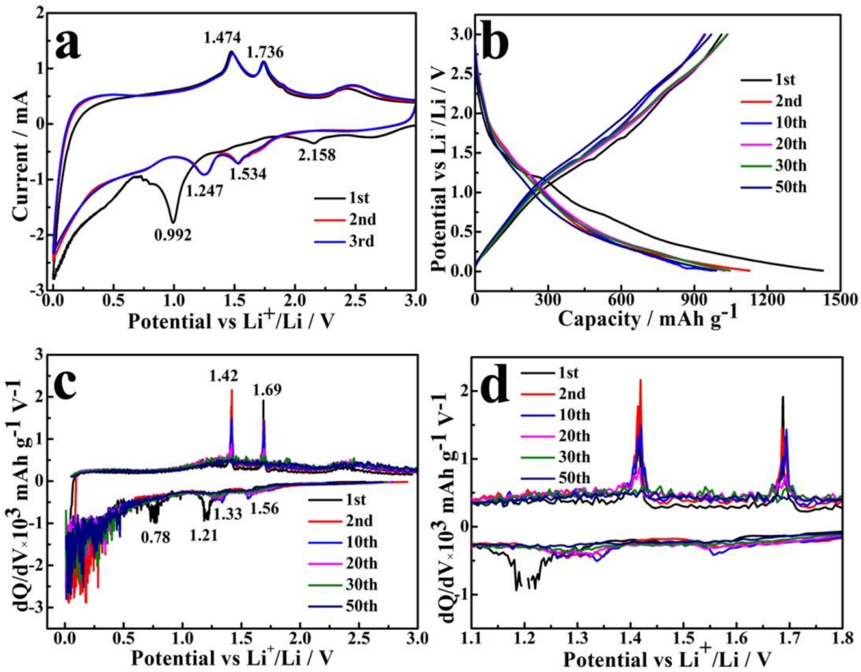

Figure 4. (a) CV curves of MoO_2-Cu@NC electrodes for the first three cycles at a scan rate of 0.2 mV s^{-1},(b) Discharge–charge curves of MoO_2-Cu@NC electrodes at 0.1 A g^{-1}, (c) Differential capacity versus voltage curves of MoO_2-Cu@NC electrodes and (d) Magnified image of dQ/dV curves

To gain insight into the lithium storage mechanism, the first three cyclic voltammetry (CV) curves of the MoO_2-Cu@NC electrodes at 0.2 mV s^{-1} in a voltage ranging from 0.0-3.0 V were shown in Fig. 4a. During the first cathodic polarization process, a sharp peak at 0.992 V indicates the phase transition from monoclinic to orthorhombic phase [19]. A wide peak at around 0.5 V can be ascribed to the irreversible reduction of the electrolyte and the formation of a solid electrolyte interface (SEI) layer, which inevitably leads to the initial capacity loss [38]. Another peak at 2.158 V disappears in the subsequent cycles, which is related to the irreversible insertion of Li^+ into superfine pores in the carbon matrix or the side reactions on the electrode surface [39]. In subsequent cycles, two pairs of peaks at (1.247/1.474 V) and (1.534/1.736 V) represent reversible electrochemical lithium intercalation /deintercalation between MoO_2 and partially lithiated $LixMoO_2$ [40, 41]. After the first cycle, the CV curves overlap well, which indicates that the discharge-charge process of MoO_2-Cu@NC electrodes is stable and reversible.

Fig. 4b shows discharge–charge curves of the MoO_2-Cu@NC electrodes at 0.1 A g^{-1}. The discharge/charge capacities of the MoO_2-Cu@NC electrodes in the first cycle are 1427.5 and 1011.6 mAh g^{-1}, and the Coulombic efficiency (CE) is 70.9%. The capacity loss may be mainly due to the irreversible capacity caused by SEI. In the 2^{nd}, 10^{th} 20^{th} 30^{th} and 50^{th} cycles, the MoO_2-Cu@NC electrodes exhibit reversible capacities of 1127.1, 973.9, 1025.4, 1045.6 and 989 mAh g^{-1}, respectively, with coulombic efficiency up to ~98%.

In addition to common CV and charge/discharge analyses, differential capacity analysis can also be used to obtain more information on the electrochemical behaviour of the MoO_2-Cu@NC electrodes. This technique demonstrates the relationship between the capacity change dQ / dV and the voltage V. Fig. 4c displays the corresponding differential capacity curves of MoO_2-Cu@NC electrodes in particular cycles, which are derived from charge/discharge curves in Fig. 4b. As shown, two pairs of reduction/oxidation peaks were observed due to the phase transitions of MoO_2-Cu@NC electrodes during lithium insertion and extraction process, which is consistent with CV results except the redox peaks shift slightly to lower potential. It is obvious that the intensity of the differential capacity peaks decreases gradually with increasing numbers of cycles, (shown in Fig. 4d). Two pairs of reduction/oxidation peaks almost disappear after 30 cycles although the discharge capacity is still maintained at 1045.6 mAh g-1 in the 30^{th} cycle. This phenomenon demonstrates that the lithiation mechanism of MoO_2-Cu@NC electrode has changed during the cycle. It can be deduced from the dQ/dV curves that the main contribution in the total capacity maybe is electric double layer capacity with increasing cycle number. Further studies on mechanism of charging and discharging of MoO_2-Cu@NC nanocomposite electrode are in progress.

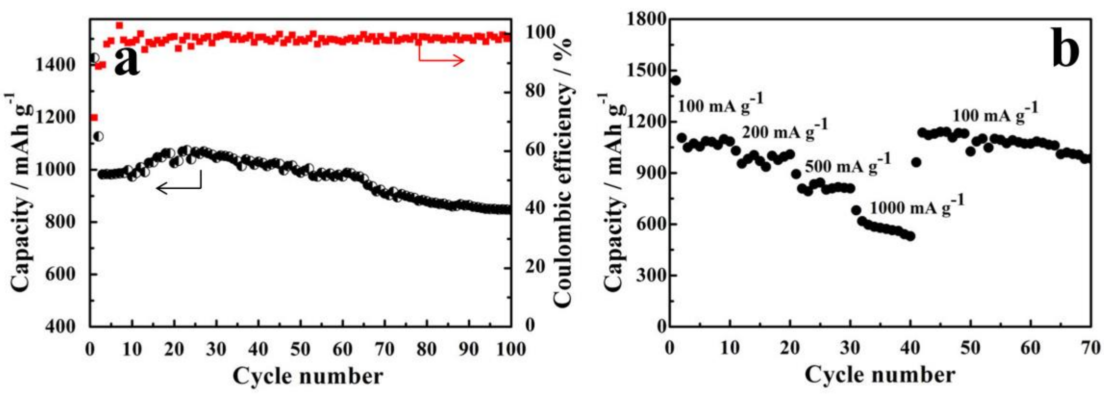

Figure 5. (a) Cycle stability of MoO_2-Cu@NC electrodes and (b) Rate capability test for the MoO_2-Cu@NC electrodes at various current densities

Cycling stability is crucial for LIBs applications. Fig. 5a displays the cycling stability of the MoO_2-Cu@NC electrodes at 100 mA g^{-1}. An initial charge capacity is 1427.5 mAh g^{-1} for MoO_2-Cu@NC electrodes. However, the discharge capacity is only 1127.1 mA h g^{-1} at the second cycle. The initial capacity loss was attributed to the decomposition of the electrolyte and the formation of the SEI film. Then, the discharge capacity gradually increases to 1074 mAh g^{-1} in the subsequent cycles. After 100 cycles, the specific capacity remains 846.1 mAh g^{-1} with 78.8% capacity retention. After the first few cycles, the coulombic efficiency approaches 100%. The MoO_2-Cu@NC electrodes also present an excellent rate performance. It can be seen from Fig. 5b that the average specific capacities of the MoO_2-Cu@NC electrodes are about 1086, 1001, 810, and 580 mAh g^{-1} at 100, 200, 500, and 1000 mA g^{-1}, respectively. The capacity of the MoO_2-Cu@NC electrodes quickly recovers to as high as 1136 mA h g^{-1} when the current density is reduced to 100 mA g^{-1}. The electrochemical performance is higher in this work than that of most MoO_2 electrode materials reported (Table 1) [42-49]. The improved performance may be due to the homogeneous carbon coating and the coexistence of Cu nanocrystallites, which improves electronic conductivity and relieves the volume change during lithium insertion extraction processes. Moreover, the presence of nitrogen in the MoO_2-Cu@NC nanocomposites could increase the active sites and the electronic conductivity for Li insertion/extraction, further improving the electrochemical performance of MoO_2-Cu@NC nanocomposites [50].

Table 1. Comparison of lithium-storage performance of different MoO_2/carbon composites

materials	SC (mAh g^{-1})	Cycle Number	Current (mA g^{-1})	Rate capability		Ref.
				SC (mAh g^{-1})	Current (mAg^{-1})	
Cu@MoO_2@C	724	140	100	637	500	[42]
MoO_2/C	677.4	80	100	455	1000	[43]
MoO_2-Cu/C	699.7	100	100	830	500	[26]
MoO_2/C	784.7	60	100	707.7	200	[19]
MoO_2	780	40	100	673.8	500	[6]
MoO_2/Mo_2CT_x	820	100	100	561	2000	[44]
MoO_2/NC	692.4	100	500	610	1000	[45]
MoO_2/NC	708	100	100	678	500	[29]
MoO_2 NR	830	29	42	260	838	[46]
MoO_2/rGO	801	50	100	400	1000	[47]
MoO_2/C	800	300	100	700	500	[48]
MoO_2/Ni/C	618	50	100	463	1000	[49]
MoO_2-Cu@NC	846	100	100	810 580	500 1000	This work

Note: SC: specific capacity; rGO: reduced grapheme oxide; NC: nitrogen-doped carbon.

4. CONCLUSION

In summary, the MoO_2-Cu@NC nanocomposites consisting of MoO_2 nanoparticles, nitrogen-doped carbon and Cu nanocrystallites have been successfully synthesized via a facile room temperature solution-phase route followed with simple thermal treatment. The Cu nanocrystallites can improve the electrical conductivity of the composite materials for fast charge transfer. Nitrogen-doped carbon can buffer the volume change and provide more active sites for Li insertion/extraction. Benefiting from the unique structure, the MoO_2-Cu@NC nanocomposites exhibit excellent cycling stability (846 mA h g^{-1} after 100 cycles at 100 mA g^{-1}) and improved rate performance (580 mA h g^{-1} at 1000 mA g^{-1}). Furthermore, differential capacity analysis demonstrates that the lithiation mechanism of MoO_2-Cu@NC electrode has changed during the cycle for the first time. The work also proposes a facile synthetic strategy of metal oxide/carbon nanocomposite with co-doping of Cu and nitrogen for high-capacity lithium ion batteries.

ACKNOWLEDGEMENTS

This work was supported by the financial support of the technical innovation major project of Hubei Province (No.2017ABA155) and the central committee guides local science and technology development special project of Hubei Province (No. 2018ZYYD062).

References

1 C. Zhao, C. Yu, M. Zhang, H. Huang, S. Li, X. Han, Z. Liu, J. Yang, W. Xiao, J. Liang, X. Sun and J. Qiu, *Adv. Energy. Mater.*, 7(2017), 1602880.
2 Y.-X. Wang, J. Yang, S.-L. Chou, H. K. Liu, W.-X. Zhang, D. Zhao and S. X. Dou, *Nat. Commun.*, 6(2015), 9689.
3 Z. C, M. Qu, J. Shi, H. Z. Wu, Y. C. Liu, J. T. Jiang and C. Yan, *J. Power Sources*, 410-411(2019), 179-187.
4 M. Idrees, S. Batool, J. Kong, Q. Zhuang, H. Liu, Q. Shao, N. Lu, Y. Y. Feng, E. K. Wujcik, Q. Gao, T. Ding, R. B. Wei and Z. H. Guo, *Electrochim. Acta*, 296(2019), 925-937.
5 R. Li, X. Zhu, Q. Fu, G. Liang, Y. Chen, L. Luo, M. Dong, Q. Shao, C. Lin, R. Wei and Z. Guo, *Chem. Commun.*, 55(2019), 2493-2496.
6 Y. Y. Yao, J. C. Zheng, Z. Y. Gong, Z. Y. Ding, J. Zhang, W. J. Yu, D. A. M. Bengono, H. Li, B. Zhang and H. Tong, *J. Alloy. Comp.*, 790(2019), 288-295.
7 S. Tang, C. Shen, W. Ji, J. Liu and D. Fichou, *Mater. Res. Bull.*, 91(2017), 85-90.
8 H. Liu, J.-G. Wang, W. Hua, J. Wang, D. Nan and C. Wei, *Chem. Eng. J.*, 354(2018), 220-227.
9 X. Hu, W. Zhang, X. Liu, Y. Mei and Y. Huang, *Chem. Soc. Rev.*, 44(2015), 2376-2404.
10 D. Larcher, G. Sudant, J. B. Leriche, Y. Chabre and J. M. Tarascon, J. Electrochem. Soc., 149(2002), A234.
11 J. H. Ku, Y. S. Jung, K. T. Lee, C. H. Kim and S. M. Oh, *J. Electrochem. Soc.*, 156(2014), A688-A693.
12 X. Liu, D. Wu, W. Ji and W. Hou, *J. Mater. Chem. A* , 3(2015), 968 – 972.
13 Y. M. Sun, X. L. Hu, W. Luo and Y. H. Huang, *ACS Nano*, 5(2011), 7100-7107.
14 X. Wang, Y. Xiao, J. Wang, L. Sun and M. Cao, *J. Power Sources*, 274(2015), 142-148.
15 L. Chen, H. Jiang, H. Jiang, H. Zhang, S. Guo, Y. Hu and C. Li, *Adv. Energy Mater.*, 7(2017), 1602782.
16 Z. Xiu, D. Kim, M. H. Alfaruqi, J. Song, S. Kim, P. T. Duong, V. Mathew, J. P. Baboo and J. Kim, *J. Alloy. Comp.*, 696(2017), 143-149.
17 J. Ni, Y. Zhao, L. Li and L. Mai, Nano Energy, 11(2015), 129-135.
18 H. J. Zhang, J. Shu, K.-X. Wang, X.-T. Chen, Y.-M. Jiang, X. Wei and J.-S. Chen, *J. Mater. Chem.*, 2(2014), 80-86.
19 L. Zhou, H. B. Wu, Z. Wang and X. W. Lou, *ACS Appl. Mater. Inter.*, 3(2011), 4853-4857.
20 S. Tang, L. Yang, J. Liu and D. Fichou, *Mater. Res. Bull.*, 2018, 102, 277–281.
21 B. Y. Xia, Y. Yan, N. Li, H. B. Wu, X. W. Lou and X. Wang, Nature Energy 1(2016), 15006.

22 F. Zou, X. Hu, Z. Li, L. Qie, C. Hu, R. Zeng, Y. Jiang and Y. Huang, *Adv. Mater.*, 26(2014), 6622-6628.
23 Y. Yang, Z. Lun, G. Xia, F. Zheng, M. He and Q. Chen, *Energy Environ. Sci.*, 8(2015), 3563–3571.
24 S.Li, ZG Luo, XX Cao,GZ Fang, SQ Liang, *Int. J. Electrochem. Sci.*, 13(2018), 23–28.
25 J. Qiu, M. Yu, Z. Zhang, X. Cai and G. Guo, *J. Alloy. Comp.*, 775(2019), 366-371.
26 K. Zhang, H. Yang, M. Lü, C. Yan, H. Wu, A. Yuan and S. Lin, *J. Alloy. Comp.*, 731(2018), 646-654.
27 G. Xia, D. Liu, F. Zheng, Y. Yang, J. Su and Q. Chen, *J. Mater. Chem. A*, 4(2016), 12434–12441.
28 W. Tian, H. Hu, Y. Wang, P. Li, J. Liu, J. Liu, X. Wang, X. Xu, Z. Li, Q. Zhao, H. Ning, W. Wu and M. Wu, *ACS Nano*, 12(2018), 1990-2000.
29 H. Sun, Y. Zhang, H. Liu, X. Zhang and J.-G. Wang, *J. Alloy. Comp.*, 787(2019), 45-52.
30 S. Niu, Z. Wang, T. Zhou, M. Yu, M. Yu and J. Qiu, *Adv. Funct. Mater.*, 27(2017), 1605332.
31 J. Xu, L. Wu, T. Guo, G. Zhang, C. Wang, H. Li, X. Li, V. Singh, W. Chen, R. Gref and J. Zhang, *Int. J. Pharm.*, 556(2019), 89-96.
32 V. V. T. Padil and M. Černík, *Int. J. Nanomed*, 8(2013), 889-898.
33 L. Zeng, X. Huang, X. Chen, C. Zheng, R. Liu, G. Chen, Q. Qian, Q. Chen and M. Wei, *RSC Adv.*, 6(2016), 105558–105564.
34 F. F. Xia, X. L. Hu, Y. M. Sun, W. Luo and Y. H. Huang, *Nanoscale*, 4(2012), 4707-4711.
35 H. Li, C. Lu and B. Zhang, *Electrochim. Acta* , 120(2014), 96-101.
36 Y. Shi, S. L. Chou, J. Z. Wang, D. Wexler, H. J. Li, H. K. Liu and Y. Wu, *J. Mater. Chem.*, 22(2012), 16465-16470.
37 G. Chen, L. Zhang, Y. Zhang, K. Liu, Z. Long and Y. Wang, *J. Mater. Chem. A*, 7(2019), 7194–7201.
38 M. V. Reddy, T. Yu, C. H. Sow, Z. X. Shen, C. T. Lim, G. V. SubbaRao and B. V. R. Chowdari, *Adv. Funct. Mater.*, 17(2007), 2792.
39 G. Liu and J. Shao, *J Mater Chem. A*, 5(2017), 9801-9806.
40 S. Hu, F. Yin, E. Uchaker, W. Chen, M. Zhang, J. Zhou, Y. Qi and G. Cao, *J. Phys. Chem.*, 2014, C, 24890-24897.
41 X. Zhang, X. Song, S. Gao, Y. Xu, X. Cheng, H. Zhao and L. Huo, *J. Mater. Chem. A* 2013, 1, 6858-6864.
42 X.-y. Li, Q.-g. Xiao, Y.-y. Gao, H.-l. Zhang, H.-b. Xu and Y. Zhang, *J. Alloy. Comp.*, 723(2017), 1113-1120.
43 J. Min, K. Wang, J. Liu, Y. Yao, W. Wang, L. Yang, R. Zhang and M. Lei, *J. Power Sources*, 363(2017), 392-403.
44 S. Petnikota, K. W. Teo, L. Chen, A. Sim, S. K. Marka, M. V. Reddy, V. Srikanth, S. Adams and B. Chowdari, *ACS. Appl. Mater. Inter.*, 8(2016), 10884-10896.
45 X. Tan, C. Cui, S. Wu, B. Qiu, L. Wang and J. Zhang, *Chem. Asian J.* , 12(2016), 36-40.
46 Q. Xia, H. Zhao, Z. Du, Z. Zhang, S. Li, C. Gao and K. Swierczekc, *J. Mater. Chem. A*, 4(2016), 605-611.
47 L. Zhang, W. He, M. Ling, K. Shen, Y. Liu and S. Guo, *J. Alloy. Comp.*, 768(2018), 714-721.
48 C. Xia, D. B. Velusamy, A. A. Farah, P. Li, Q. Jiang, I. N. Odeh, Z. Wang, X. Zhang and H. N. Alshareef, *Nano Lett.*, 18(2018), 1506-1515.
49 Y. Zhu, S. Wang, Y. Zhong, R. Cai, L. Li and Z. Shao, *J. Power Sources*, 307(2016), 552-560.
50 L. C. Yang, W. Sun, Z. W. Zhong, J. W. Liu, Q. S. Gao, R. Z. Hu and M. Zhu, *J. Power Sources*, 306(2016), 78-84.

© 2020 The Authors. Published by ESG (www.electrochemsci.org). This article is an open access article distributed under the terms and conditions of the Creative Commons Attribution license (http://creativecommons.org/licenses/by/4.0/).